The Influence of Wind Speed on Shallow Marine Cumulus Convection

LOUISE NUIJENS*

Department of Atmospheric and Oceanic Sciences, University of California, Los Angeles, Los Angeles, California

BJORN STEVENS

Max Planck Institute for Meteorology, Hamburg, Germany

(Manuscript received 30 December 2010, in final form 21 July 2011)

ABSTRACT

The role of wind speed on shallow marine cumulus convection is explored using large-eddy simulations and concepts from bulk theory. Focusing on cases characteristic of the trades, the equilibrium trade wind layer is found to be deeper at stronger winds, with larger surface moisture fluxes and smaller surface heat fluxes. The opposing behavior of the surface fluxes is caused by more warm and dry air being mixed to the surface as the cloud layer deepens. This leads to little difference in equilibrium surface buoyancy fluxes and cloud-base mass fluxes. Shallow cumuli are deeper, but not more numerous or more energetic. The deepening response is necessary to resolve an inconsistency in the subcloud layer. This argument follows from bulk concepts and assumes that the lapse rate and flux divergence of moist-conserved variables do not change, based on simulation results. With that assumption, stronger winds and a fixed inversion height imply larger surface moisture and buoyancy fluxes (heat fluxes are small initially). The consequent moistening tends to decrease cloud-base height, which is inconsistent with a larger surface buoyancy flux that tends to increase cloud-base height, in order to maintain the buoyancy flux at cloud base at a fixed fraction of its surface value (entrainment closure). Deepening the cloud layer by increasing the inversion height resolves this inconsistency by allowing the surface buoyancy flux to remain constant without further moistening the subcloud layer. Because this explanation follows from simple bulk concepts, it is suggested that the internal dynamics (mixing) of clouds is only secondary to the deepening response.

1. Introduction

The ''trades'' owe their name to the easterly surface winds that prevail over subtropical oceans and that once made foreign commerce flourish. Within the trades, widespread fields of shallow cumulus dominate the various forms of moist convection. These trade wind cumuli remain shallow as their growth is halted by the trade inversion, limiting their depth to typically 1 or 2 km (Malkus 1956; Stevens 2005). It is not uncommon, however, to find cumuli that reach up to 3 or 4 km (Medeiros et al. 2010) and that produce considerable rain showers (Nuijens et al. 2009).

In studying what controls the behavior of these clouds, the role of the trade winds themselves, from which the region derives its original name, has received far less attention compared to other features, such as large-scale divergence, sea surface temperature, and the thermodynamic structure of the lower troposphere. Although it is understood that the winds are crucial, by inducing evaporation from the ocean's surface, their persistent nature may have encouraged us to take them for granted. Exactly how and how much the weakening and strengthening of the trades, as measured by wind speed, affects its clouds has not been extensively studied. In finescale modeling studies of shallow cumulus convection, for instance, wind speed is commonly prescribed as a constant forcing.

The objective of our work is to gain more insight into the influence of wind speed on cloud properties, turbulent fluxes, and the structure of the trade wind layer. For cases characteristic of the trades, large-eddy simulation (LES) is used to study the response of convection to perturbations in wind speed. In addition, bulk theoretical

* Current affiliation: Max Planck Institute for Meteorology, Hamburg, Germany.

Corresponding author address: Louise Nuijens, Max Planck Institute for Meteorology, Bundesstrasse 53, 20146 Hamburg, Germany. E-mail: louise.nuijens@zmaw.de

DOI: 10.1175/JAS-D-11-02.1

concepts are used to help us understand the behavior observed in the simulations.

The motivation for having a closer look at wind speed stems from a previous study that used observations collected during the Rain in Cumulus over the Ocean (RICO) field campaign to analyze relationships among clouds, precipitation, and the large-scale meteorological environment (Nuijens et al. 2009). Results from that study suggest that wind speed, in addition to subsidence, plays a major role in regulating variability in boundary layer humidity, and hence in cloudiness and rainfall. More specifically, stronger winds are observed to correspond to higher humidity throughout the entire boundary layer and an increase in area rainfall. The hypothesized mechanism behind this relationship that we wish to test is that stronger winds lead to enhanced evaporation, more upward mixing of moisture by clouds, and an increase of humidity in the cloud layer. This in turn favors the development of deeper clouds with more liquid water, which may rain more.

Relationships among wind speed, humidity, and rainfall are not new in studies of deep convection and the ideas explaining such relationships are similar to what is proposed for shallow convection. By compositing sounding profiles over the island of Nauru in the western tropical Pacific, Holloway and Neelin (2009) show that variability in deep convective rainfall is mainly linked to variability in free tropospheric humidity. They attribute the increase in rainfall with humidity to an increase in the buoyancy of cloudy updrafts, via entrainment. Similar findings are discussed in Bretherton et al. (2004) and Back and Bretherton (2005), who also show that wind speed explains a significant part of the variability in daily rainfall in the Pacific ITCZ from four years of satellite-retrieved data.

One idea proposed in these studies is that enhanced evaporation under stronger winds leads to a greater number of shallow cumuli, where each cumulus contributes to a moistening and deepening of the boundary layer (here including both the subcloud and cloud layer), which increases the chance that a deeper precipitating system develops. Interpreting the RICO results in view of these ideas, a few interesting questions arise: Does an increase in wind speed just lead to a greater number of shallow cumuli or to a deepening of cumuli in general? How does that impact the moistening versus the deepening of the boundary layer? Given that the layer close to the ocean surface moistens, can the enhanced evaporation be sustained over a longer period of time?

The approach that we use in addressing these questions is inspired by the observations that motivated our study. The vertical structure observed during RICO at a single point reflects the history of air masses that have traveled for a few days through the trades at a certain wind speed. During this time the different processes that act on the layer (the surface fluxes of heat and moisture, subsidence, and radiation) may have reached equilibrium. The increase in boundary layer humidity with wind speed may thus be explained as an equilibrium response to stronger winds. This approach is further explained in section 2. In section 3, the simulations that are used to describe the transient response to wind speed perturbations, as well as the equilibrium response, are described. We focus on nonprecipitating shallow cumulus cases that have an idealized thermodynamic structure, though not far from what is typically observed within the trades. Excluding rainfall may seem at odds with our motivation, but our goal here is to understand the response of clouds to wind speed first, and rain may blur part of that response. Following the simulations, we apply concepts from bulk (equilibrium) theory, such as those described in Betts and Ridgway (1989), to help understand how the underlying conservation equations constrain the equilibrium response of the trade wind layer (section 4). The results are discussed in section 5 and conclusions are summarized in section 6.

2. The idea

Imagine that the vertical profiles in the top panel of Fig. 1 represent the vertical structure of air masses that have traveled a few days through the trades. If the wind shear that is present in the profile of u is ignored, one assumes that the air masses have been advected in their entirety by a mean (surface) wind speed U. An idealized picture of the vertical structure at low U (dashed lines) is shown in the bottom panel. It exhibits a structure that is typical for the trades: a well-mixed layer of depth η above the ocean's surface, the cloud layer that is less rapidly mixed, and an inversion layer at h that separates the turbulent boundary layer from the free tropospheric air above it.

This thermodynamic structure results from a subtle balance between the processes that act on the layer, among which clouds are an important link. It is useful to consider the equilibrium state of the layer because this eliminates the time derivative from the underlying conservation laws and allows one to directly link the gradients of temperature and humidity to the processes at play. The equilibrium state for a nonprecipitating case follows from the tendency equations of the conserved variables θ_l and q_t (the liquid water potential temperature and total specific humidity), with the time derivatives $\partial\theta_l/\partial t$ and $\partial q/\partial t$ put to zero:

$$0 = -\overline{w}\frac{\partial\theta}{\partial z} + Q_r - \frac{\partial F_\theta}{\partial z}, \tag{1}$$

$$0 = -\overline{w}\frac{\partial q}{\partial z} - \frac{\partial F_q}{\partial z}, \tag{2}$$

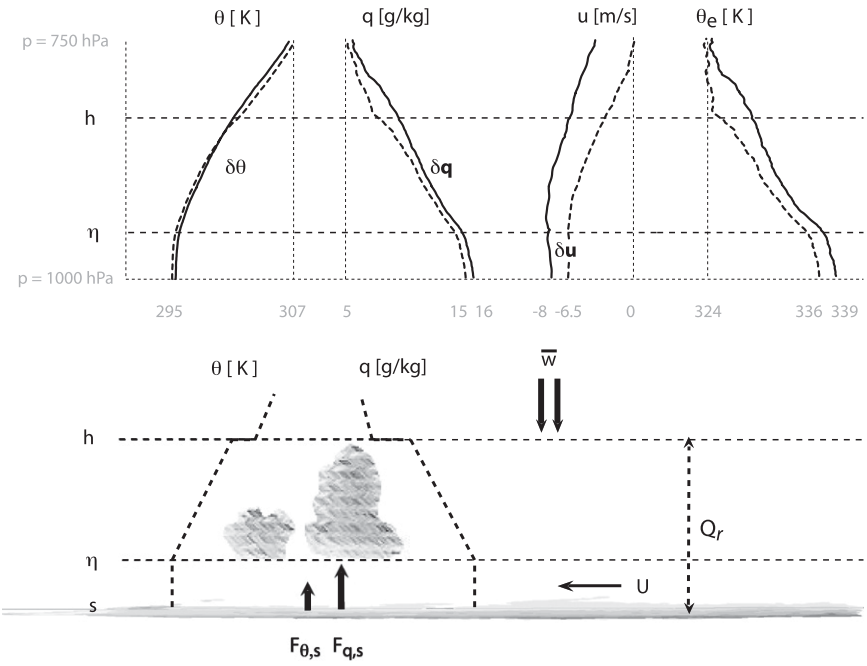

FIG. 1. (top) Composite profiles of θ, q, u, and θ_e conditioned on periods with little rainfall (dashed lines) and periods with moderate rainfall (solid lines) as observed during RICO [adapted from Fig. 7 in Nuijens et al. (2009)]. (bottom) An idealization of the θ and q profiles of the first composite (with little rainfall and lower zonal wind speeds), along with subsidence $\overline{w}$, radiative cooling Q_r, and the surface fluxes of heat $F_{\theta,s}$ and moisture $F_{q,s}$.

where for convenience q_t is written as q and θ_l is written as θ. It is assumed that the air mass is horizontally homogeneous (which eliminates the horizontal advection terms) and that there is no significant lateral advection into the air mass. The term Q_r denotes an imposed cooling, which represents radiative processes; $\overline{w}$ is the subsidence velocity ($\overline{w} < 0$); and $F_\theta = \overline{w'\theta'}$ and $F_q = \overline{w'q'}$ denote the turbulent fluxes of θ and q, respectively. In stationarity, conservation of energy (in this case conservation of θ_l) requires that anywhere between the surface s and the inversion h, warming due to subsidence (acting on the temperature gradient) and due to the turbulent heat flux divergence balances the imposed cooling. Moisture conservation requires that drying due to subsidence balances moistening due to the turbulent moisture flux divergence.

Wind speed enters the above equations via the surface fluxes. These are typically modeled with bulk formulas (Fairall et al. 2003), wherein the flux of any quantity is the product of wind speed and the difference of that quantity between the surface and the subcloud layer (for θ and q):

$$F_{\theta,s} = C_D U(\theta_s - \theta_m), \tag{3}$$

$$F_{q,s} = C_D U(q_s - q_m). \tag{4}$$

Here, m denotes the well-mixed subcloud layer, C_D is a surface transfer coefficient derived from similarity theory, and $U = \sqrt{u_m^2 + v_m^2}$ is the wind speed above the surface; also, θ_s is the sea surface temperature (SST) and q_s is the saturation specific humidity at SST. The surface fluxes combined give the surface buoyancy flux $F_{b,s}$:

$$F_{b,s} \simeq \frac{g}{\theta_{v,0}}(F_{\theta,s} + \epsilon\theta F_{q,s}), \tag{5}$$

where $g = 9.81$ m s^{-2} is the gravitational acceleration, $\theta_{v,0}$ is the basic-state virtual potential temperature, and $\epsilon = (R_v/R_d) - 1 = 0.608$, where $R_v = 461.5$ J kg^{-1} and $R_d = 287$ J kg^{-1} are the gas constants for water vapor and dry air.

Equations (3) and (4) show that if U is perturbed by δU, the surface fluxes change directly, which changes θ_m and q_m [Eqs. (1) and (2)] and asks for a further adjustment of the surface fluxes. If warming and moistening close to the surface (which decreases $\theta_s - \theta_m$ and $q_s - q_m$) is sufficient, it can offset the effect of stronger winds on the fluxes, so that the equilibrium surface fluxes remain unchanged: $\delta F_q, \delta F_\theta \approx 0$. If moistening and warming are not sufficient, the surface fluxes in a new equilibrium will be different and $\delta F_q, \delta F_\theta \neq 0$.

In the following section we explore the issue with LES, where one of our main findings is that a change in wind speed leads to a change in the depth of the layer

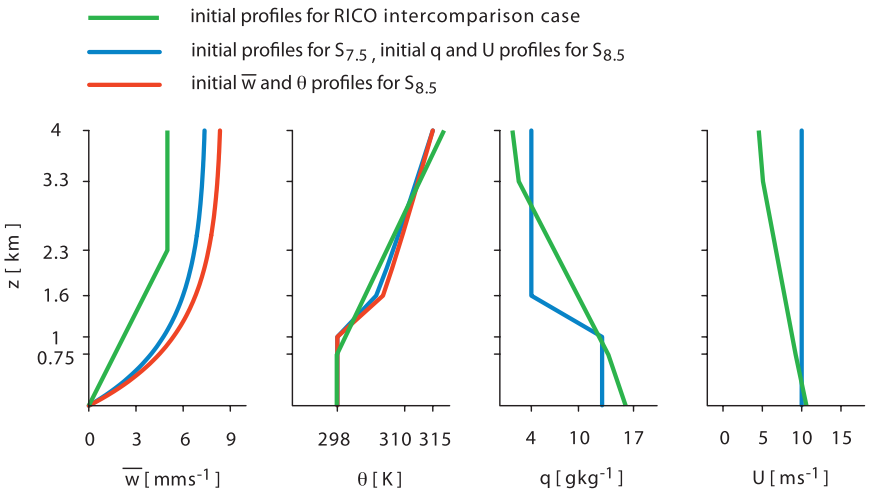

FIG. 2. (left) Vertical profile of subsidence velocity and the initial profiles of (left middle) liquid water potential temperature , (right middle) specific humidity, and (right) wind speed $U = \sqrt{u^2 + v^2}$ for the RICO intercomparison case (green; Van Zanten et al. 2011), the $S_{7.5}$ case (blue), and the $S_{8.5}$ case, which only differs from $S_{7.5}$ in its profile of $\overline{w}$ and θ (red).

h, with δF_q, $\delta F_\theta \neq 0$. By using some of the above bulk concepts in section 5, we demonstrate that this deepening of the cloud layer with stronger winds is a necessary adjustment of the layer to a new equilibrium. We also explain why the solution we hypothesized in our previous study (Nuijens et al. 2009) whereby h does not change and δF_q, $\delta F_\theta = 0$, is inconsistent.

3. Large-eddy simulation

a. Simulation setup

All the simulations are performed with the University of California, Los Angeles (UCLA) LES code described in Savic-Jovcic and Stevens (2008), except for the time stepping, which is performed with a Runge–Kutta-3 scheme (with an adaptive time step limited to be no larger than 1 s). The simulations are performed with initial and boundary conditions that lead to the development of typical shallow cumulus convection after a few hours of spinup (Fig. 2; Table 1). The simulation setup we initially explore is that of the RICO LES intercomparison case, which derives its initial profiles from measurements during the RICO field study and its large-scale forcings from regional downscaling of European Centre for Medium-Range Weather Forecasts (ECMWF) ReAnalyses (Van Zanten et al. 2011). The RICO case does not achieve stationarity (the boundary layer continues to deepen during the simulation); it has a significant amount of wind shear (the geostrophic profile of u is sheared by 8 m s^{-1} over 4 km) and allows rain to develop. The lack of stationarity complicates the analysis and both wind shear and rain provide additional mechanisms that can influence the dynamics of the layer and that we prefer to exclude. For these reasons, we turn our focus to a framework introduced by Bellon and Stevens (2012, hereafter BS12), which prescribes large-scale forcings and initial profiles that are not uncommon for the subtropics but are further idealized relative to the RICO case (Fig. 2; Table 1). We here give a short outline of the (dis)similarities between the two case setups, in addition to a more detailed specification of the BS12 framework

TABLE 1. Initial and boundary conditions, forcings, and other specifications for the idealized framework by BS12. Details are given in the text.

Case	$S_{7.5}$, $S_{8.5}$
Forcings	
$\overline{w}_0$ (m s^{-1})	7.5×10^{-3}, 8.5×10^{-3}
H (m)	1000
Q_r (K day^{-1})	2.5
u_g (m s^{-1})	10
v_g (m s^{-1})	0
Initial and boundary conditions	
SST (K)	300
q (g kg^{-1})	$z < 1$ km: 13
	$z \geq 1.6$ km: 4
θ (K)	$z < 1$ km: 298
	$z \geq 1.6$ km: $d\theta/dz = Q_r/\overline{w}$
Domain and resolution	
Δt (s)	1
Δx, Δy, Δz (m)	$50 \times 50 \times 25$*
nx, ny, nz (nondimensional)	$256 \times 256 \times 190$
Domain size (km)	$12.8 \times 12.8 \times 5$

* At $z > 4$ km vertical grid is stretched uniformly by a factor of 1.02.

[for a detailed description of the RICO case we refer the reader to Van Zanten et al. (2011)].

Both the RICO case and the idealized case support an Eulerian reference frame with large-scale forcings that are constant in space and time. The absence of the typical increase of SST and decrease in subsidence along a trade wind trajectory allows us to study the effect of wind speed alone. In the RICO case the subsidence profile is specified to be piecewise linear and this is generalized to a smoother exponential form in the BS12 framework (Fig. 2, left). For the RICO case a cooling tendency due to horizontal advection is combined with the radiative cooling to give a constant (with height) net cooling rate of 2.5 K day^{-1}. For our more idealized case the same cooling rate is applied. In the RICO case an additional large-scale drying tendency is applied, which is absent in the idealized case. At the surface, a prescribed SST and a slip/no-penetration condition are used, with surface thermodynamic and momentum fluxes parameterized with bulk aerodynamic formulas [see Eqs. (3) and (4)].

In the idealized case the exponential profile $\overline{w}$, such that

$$\overline{w}(z) = \overline{w}_0(1 - e^{-z/H}), \tag{6}$$

is coupled to the temperature lapse rate in the free troposphere, which follows from the assumption that subsidence warming equals radiative cooling:

$$d\theta/dz(z) = Q_r/\overline{w}(z), \tag{7}$$

where the base subsidence rate w_0 equals either 7.5 mm s^{-1} (case $S_{7.5}$), or $w_0 = 8.5$ mm s^{-1} (case $S_{8.5}$). The term H, the scale height, equals 1 km (Table 1). Although $w_0 = 7.5$ mm s^{-1} is much higher than what is typical for the trade wind regime and than what is used for RICO (where $\overline{w}$ is at most 5 mm s^{-1}), it helps compensate for the lack of a separate representation of large-scale advective tendencies and thus promotes the development of stationary solutions. In particular, the increased subsidence at the height of the inversion mimics the effect of advecting a sloped inversion, which induces strong warming and drying tendencies at that level. The use of a larger value for the subsidence also accommodates a stronger cooling rate that helps offset the lack of a separate term representing the advective cooling within the subcloud layer.

Although our case is idealized, the general behavior mimics what is evident in the less idealized RICO case. Our additional idealizations primarily act to bring us closer to a regime where equilibrium responses are found. This facilitates the analysis (as it allows us to collect statistics from the simulations over a longer period). Nonetheless, it remains interesting to see how the results generalize as some of the constraints associated with our idealizations are relaxed. In particular there is some indication that by allowing radiation to be interactive and by decoupling subsidence and the free tropospheric lapse rate (Betts and Ridgway 1989) a broader range of responses can be found.

The initial profiles of temperature and humidity in the idealized case are well mixed and constant with height up to 1 km, with $\theta = 298$ K and $q = 13$ g kg^{-1}, topped by an inversion layer that extends up to 1.6 km. Above that height, θ follows from Eq. (7), and to ensure a zero drying tendency in the free troposphere the humidity gradient is set to zero with $q = 4$ g kg^{-1}. The initial wind profile equals the geostrophic wind that is constant with height, with a zonal component of 10 m s^{-1} and a meridional component that is 0 m s^{-1} (Fig. 2). The domain is $12.8 \times 12.8 \times 5$ km^3 with a grid spacing of 50 m in the horizontal and 25 m in the vertical, stretching by a factor of 1.02 in the region where $z >$ 4 km (this is twice the horizontal and roughly twice the vertical resolution of the RICO case). Simulations are performed without rain microphysics, which removes another uncertainty, given that clouds and especially rain still exhibit a significant sensitivity to the numerical representation of the flow (Matheou et al. 2011).

The influence of wind speed is studied by perturbing the zonal wind profile by ±50%. For the RICO case this is done upon initializing the model, after which simulations are continued for 60 h. For the idealized case, the simulation strategy is slightly different. The model is first run for 60 h at a 10 m s^{-1} wind speed, during which the boundary layer approaches stationarity, after which wind speed is perturbed and the simulations are continued for another 48 h.

In order not to develop systematic numerical differences between the simulations, the Galilean transform [which is commonly used to reduce numerical dissipation and to lower the Courant–Friedrich–Levy (CFL) number in LES] is adjusted accordingly. For the RICO case the Galilean velocity equals the zonal wind speed near cloud base (acting to reduce the numerical dissipation only near this height). For the idealized framework the Galilean velocity equals the (constant with height) zonal wind. Any remaining differences in numerical advection speed left between the wind speed cases are located in the subcloud layer, once shear develops (with more shear present in simulations with stronger winds). Test simulations with different CFL numbers show that such differences do not significantly affect the conclusions we draw.

b. Perturbing wind speed

Figure 3 shows the differences in the vertical structure of the trade wind layer that have emerged after 60 h of

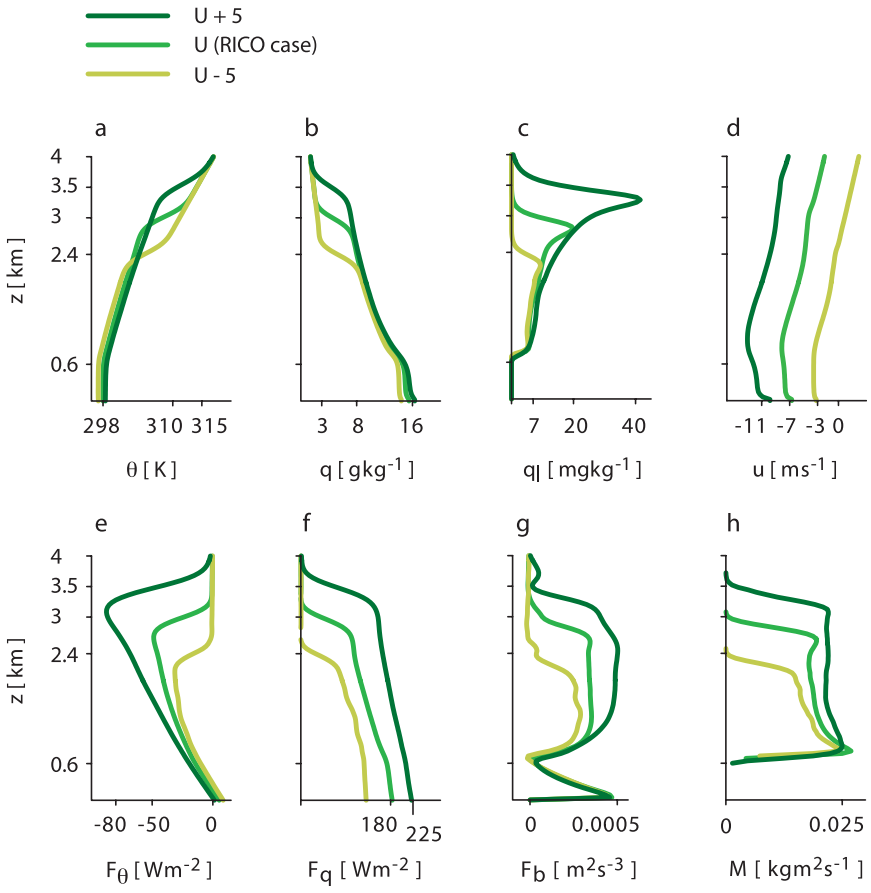

FIG. 3. The vertical profile of (a) liquid water potential temperature, (b) specific humidity, (c) liquid water, (d) zonal wind speed, (e) turbulent heat flux, (f) turbulent moisture flux, (g) buoyancy flux, and (g) mass flux for the RICO case, averaged from hour 52 to hour 60 of simulations that start with the control wind speed profile (green), $u + 5$ m s^{-1} (dark green), and $u - 5$ m s^{-1} (yellow-green).

simulating the RICO case with different initial wind profiles. At stronger winds clouds are deeper (Fig. 3c), hence the cloud layer is deeper, whereas the thermodynamic gradients have changed little (Figs. 3a,b). The subcloud layer has warmed and moistened (Figs. 3a,b), but the surface fluxes at different wind speeds remain different (Figs. 3e,f). Also interesting to note is the little difference in surface buoyancy flux and cloud-base mass flux (Figs. 3g,h). Because of wind shear and other features of the RICO case (discussed in the previous section) we continue with the idealized case for a more detailed exploration of these results. We point out that both cases do respond similarly to wind speed despite their differences in (thermo)dynamic structure, which suggests that our results are not overly sensitive to the additional idealizations introduced.

After 60 h of simulating $S_{7.5}$ and $S_{8.5}$ at a 10 m s^{-1} wind speed U_{10}, a typical trade wind layer structure has developed (Fig. 4), with a subcloud layer up to roughly 500 m and an inversion near 1.6 km for $S_{8.5}$ (red lines) and 2.3 km for $S_{7.5}$ (blue lines). Note that the Coriolis force and surface drag lead to a turning of the wind and a small amount of wind shear close to the surface (right panel). Differences in structure between $S_{7.5}$ and $S_{8.5}$ are otherwise small, with a somewhat drier subcloud layer for $S_{7.5}$, which is consistent with its boundary layer being deeper.

The boundary layer growth dh/dt for $S_{8.5}$ is zero at hour 60. This is not true for $S_{7.5}$, where the tendency to deepen the layer, as measured by $dh/dt - \overline{w}_h$, still exceeds the prescribed subsidence rate (blue lines in Fig. 5). The surface heat and moisture fluxes $F_{\theta,s}$ and $F_{q,s}$, however, are roughly constant between hour 48 and hour 60, indicating that the subcloud layer has reached stationarity. Note that $F_{\theta,s}$ is close to zero, implying that the subcloud layer temperature is equal to the sea surface temperature. Because $F_{\theta,s}$ over the ocean is typically small, the convective forcing of the layer, as measured by $F_{b,s}$, is weak and strongly influenced by $F_{q,s}$.

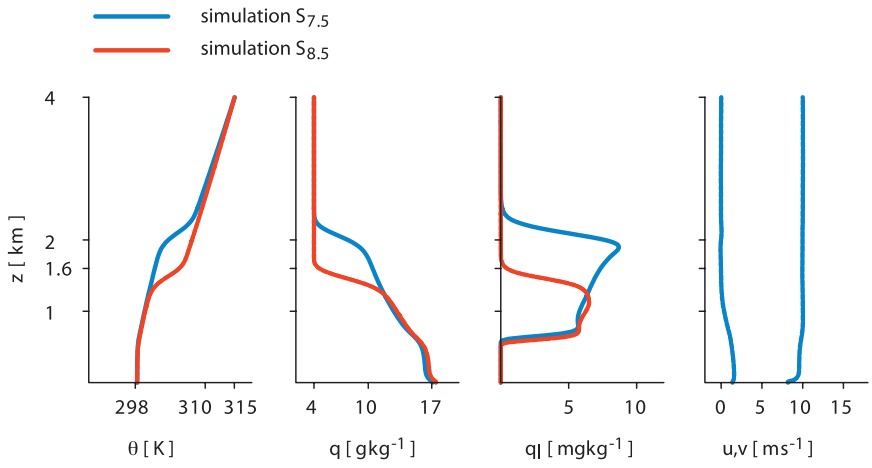

FIG. 4. The vertical profile of (left) liquid water potential temperature, (left middle) specific humidity, (right middle) liquid water, and (right) zonal and meridional wind speed for cases $S_{7.5}$ and $S_{8.5}$, averaged from hour 52 to hour 60 of the simulations.

The zonal wind speed is perturbed at hour 60 by an amount $\delta u = +5$ (U_{15}) and $\delta u = -5$ (U_5), after which all simulations, including U_{10}, are continued for two more days. The most apparent changes occur in the 6 h after the perturbation, followed by a more gradual relaxation to equilibrium (Fig. 5). Similar to the RICO simulations, the layer deepens at stronger winds, with a sudden increase in surface moisture flux and an increasingly negative surface heat flux. Cloud fraction (not shown) and the mass flux are initially perturbed but quickly relax backward to their original values. That the surface fluxes evolve more gradually throughout the simulations suggests that their evolution reflects changes in the layer structure (θ_m, q_m) after the perturbation.

The overall response is not completely linear (i.e., subtracting wind does not give the exact opposite response to adding wind). Some secondary features develop in U_{15}, such as more shear in the subcloud layer and increased cloudiness at upper levels (Figs. 6h,c), which changes its character compared to U_5 and U_{10}. The main response, however, is unaffected by these differences. One can note that the behavior of the surface heat, moisture, and buoyancy flux, as well as the mass flux, is similar to the RICO case (Figs. 3e–h), which supports the idea that the response we are seeing is general and motivates the use of the idealized case for developing our ideas. In the following analyses we focus mainly on $S_{7.5}$. Even though it does not become truly stationary at higher wind speeds, the temporal evolution is modest and steady. Moreover, because the clouds in that case get deeper they are better resolved, and in terms of the general response to a change in wind speed, $S_{7.5}$ and $S_{8.5}$ are very similar.

1) SURFACE FLUX AND DEEPENING RESPONSE

Whereas $F_{q,s}$ responds immediately to the perturbation, a direct response of $F_{\theta,s}$ is less apparent, simply because it is approximately zero to begin with (Fig. 5). Within the next hour, however, $F_{\theta,s}$ starts to decrease in U_{15} (and increase in U_5), a response that was somewhat unexpected. The reason for $F_{\theta,s}$ turning negative in U_{15} is because the layer is warming from enhanced entrainment at the top of the subcloud layer, mixing potentially warmer cloud layer air into the subcloud layer (note that $F_{\theta,s}$ is zero initially, hence the warming cannot be caused by additional surface input). The enhancement of turbulent entrainment right after the perturbation is caused by more vigorous turbulence in the subcloud layer, a result of a larger $F_{q,s}$ and $F_{b,s}$. In U_5 the opposite takes place: entrainment (warming) decreases and is less able to compensate the fixed cooling (2.5 K day^{-1}). This leads to a gradual cooling of the subcloud layer accompanied by a gradual increase in $F_{\theta,s}$.

At stronger winds, more shear develops in the subcloud layer. This occurs in a few hours after the perturbation (on a time scale much shorter than the adjustment time of the surface fluxes), and differences in near-surface wind speed among U_5, U_{10}, and U_{15} are therefore less than 5 m s^{-1} [see also the vertical profiles of u and v and of $S = \overline{u'w'}(\partial\overline{u}/\partial z) + \overline{v'w'}(\partial\overline{v}/\partial z)$ taken at the end of the simulation (Figs. 6d,h)]. Because the convective forcing in the subcloud layer is not strong to begin with, shear generation of turbulence may begin to play a more important role in U_{15}. Shear near cloud base has been shown to positively influence the rate of entrainment (Moeng and Sullivan 1994; Pino et al. 2003; Conzemius and Federovich 2006), which would imply more drying, and

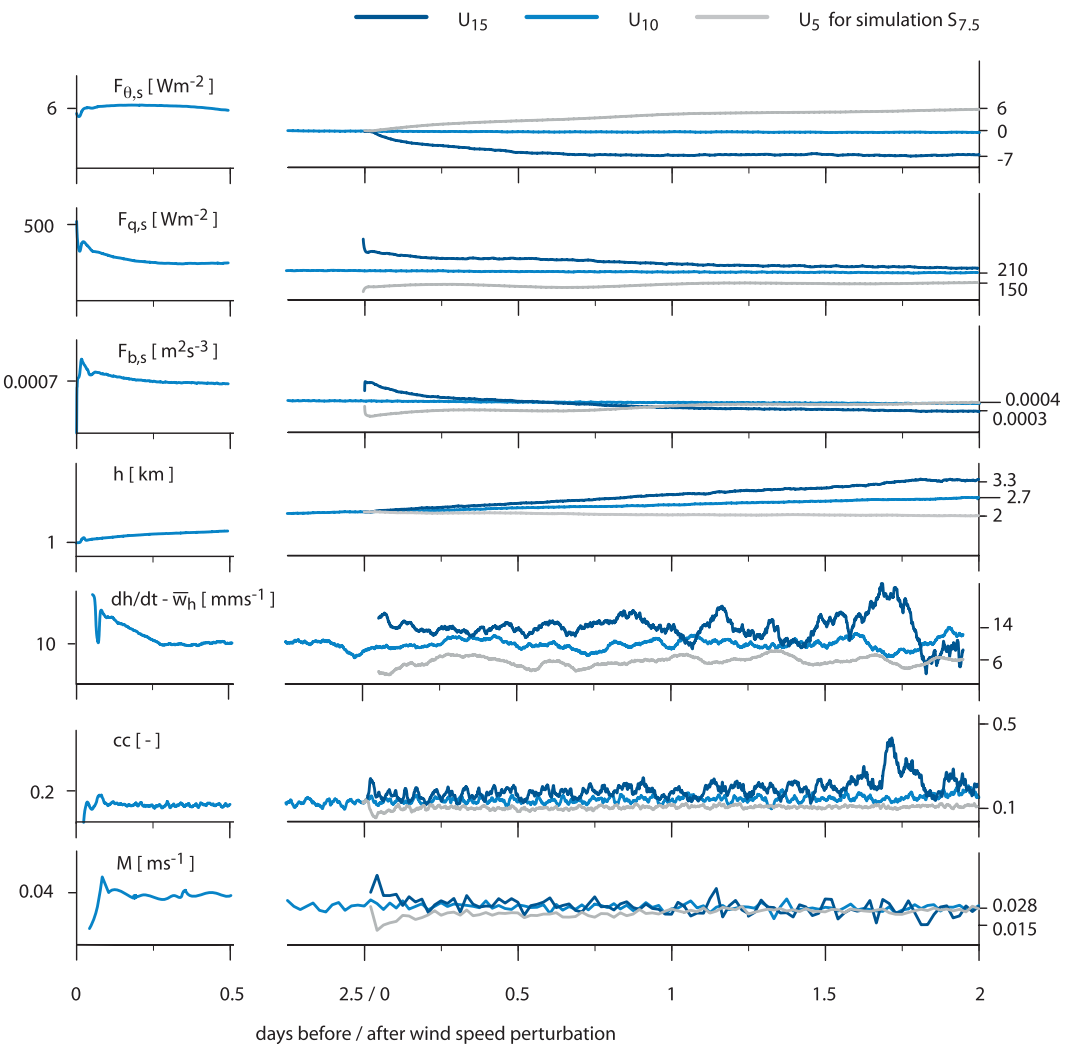

FIG. 5. Time series before and after the wind speed perturbation for case $S_{7.5}$: (from top to bottom) surface sensible heat flux, surface latent heat flux, surface buoyancy flux, boundary layer height, deepening tendency, and fraction of cloudy columns and the mass flux at cloud base for simulations U_{10} (blue), U_5 (gray), and U_{15} (dark blue).

require a larger surface moisture flux in equilibrium. Because $F_{q,s}$ in U_{15} shows more evidence of a relaxation back to its value of U_{10}, a point to which we return in the discussion (section 5), we believe such a shear effect is small and does not significantly affect the behavior of the subcloud layer.

Evidently, the wind speed perturbation, followed by a change in the surface buoyancy flux, changes the rate of mass exchange between the cloud layer and the free troposphere, as measured by $dh/dt - \overline{w}_h$. The sudden increase in $F_{q,s}$ and $F_{b,s}$ allows deeper clouds to develop that are associated with a greater flux of liquid water into the inversion. Upon mixing with the overlying dry air, liquid water evaporates, cools, and moistens the inversion, thereby slowly deepening the layer as a whole (Betts 1973; Stevens 2007; Bretherton and Park 2008). As clouds penetrate farther into the free troposphere, the net amount of dry and warm free tropospheric air that is mixed into the cloud layer increases. This additional warming and drying is felt closer to the surface, through entrainment across the subcloud and cloud layer interface. In equilibrium, this results in more input of moisture at the surface and less input of heat. The latter explains why the surface fluxes act in opposite ways and force the surface buoyancy flux to relax backward to its original value (most evident for U_5 and U_{10}).

Into the second day after the perturbation, the cases therefore have a similar surface buoyancy forcing. Cloudy updrafts are moister but also warmer, so that the liquid water flux at each level is very similar in each case. Because the layers have different depths, and the liquid water flux carried into the inversion scales with the depth

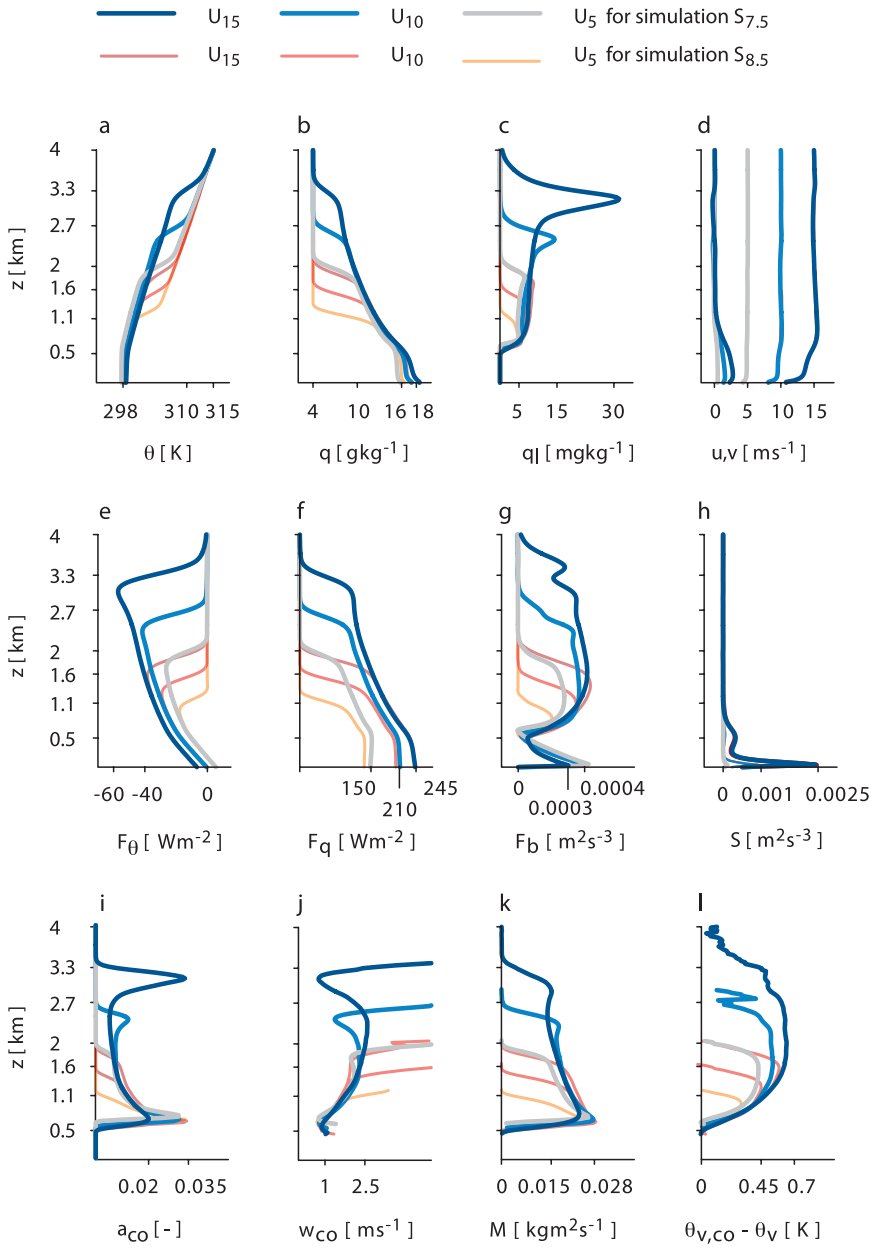

FIG. 6. Profiles of (a) liquid water potential temperature, (b) specific humidity, (c) liquid water, (d) zonal and meridional wind speed, (e) turbulent heat flux, (f) turbulent moisture flux, (g) buoyancy flux, (h) shear production of TKE, (i) cloud core fraction, (j) cloud core vertical velocity, (k) mass flux, and (l) cloud core excess of virtual potential temperature. Profiles are averaged over hours 100–108 for U_5 (gray), U_{10} (blue), and U_{15} (dark blue) for $S_{7.5}$, as well as for $S_{8.5}$ (orange, red, and dark red, respectively).

of the layer, their deepening tendencies remain different (Stevens 2007).

2) CLOUD AND MASS FLUX RESPONSE

Along with the sudden change in moisture and buoyancy flux right after the perturbation, the fraction of buoyant updrafts that reach their saturation level changes. This is evident from the sudden increase in (total) cloud cover (cc) for U_{15}, and the decrease in cc for U_5. The cloud cover, defined as the number of cloudy columns in the domain, remains altered during the simulation, but cloud fraction at cloud base (not shown), cloud-core fraction a_{co}, and the mass flux at cloud base M quickly approach values similar to that of U_{10}. The change in total

cloud cover thus reflects mainly clouds getting deeper, and because they have irregular shapes and do not necessarily fill the same column at any given height (i.e., they do not obey the maximum overlap rule), cc can change even if the vertical profile of cloud fraction does not change.

Why cloud (core) fraction changes little can be understood from the structure and dynamics of the subcloud layer. The saturation level of updrafts is typically somewhat higher than the depth of the well-mixed layer and the two are separated by a thin stable layer often called the transition layer (Malkus 1958). The transition layer is marked by a small negative jump in humidity and positive jump in temperature and reflects the penetrative nature of dry convection in the subcloud layer. When a sudden perturbation, such as an increase in wind speed, lowers the saturation level because the well-mixed layer moistens, the number of cloudy updrafts (as measured by $a_{\rm co}$) increases and along with it the mass flux:

$$M = w_{\rm co} a_{\rm co}, \tag{8}$$

where $w_{\rm co}$ is the cloud-core vertical velocity. More mass removed from the layer in turn lowers η:

$$\frac{d\eta}{dt} = E - M + \overline{w}_{\eta}, \tag{9}$$

where $\overline{w}_{\eta} < 0$ and E is the rate at which cloud layer air is entrained into the subcloud layer ($E > 0$). This mechanism ensures that η is kept close to the saturation level and reestablishes the thin transition layer. This may explain why $a_{\rm co}$ does not differ much between the wind speed cases. Note that also $w_{\rm co}$ is similar, although most evidently for U_5 and U_{10} (Fig. 6j). This can be understood if we assume that it scales with the convective velocity scale w^* (Grant and Brown 1999; Stevens 2006; Neggers et al. 2006):

$$w_{\rm co} \propto w^* = (\eta F_{b,s})^{1/3}, \tag{10}$$

where both η and $F_{b,s}$ do not change much with wind speed (as discussed earlier, because $F_{q,s}$ and $F_{\theta,s}$ respond oppositely). As a result, we observe that the mass flux is fairly constant with wind speed.

c. Toward a new equilibrium

The surface fluxes are roughly constant throughout the second day after the perturbation (Fig. 5) and the subcloud layer in U_5 and U_{10} of $S_{7.5}$, as well as in U_5, U_{10}, and U_{15} of $S_{8.5}$, are in equilibrium. Except for the two deepest cases, where boundary layer growth is not zero, the cloud and inversion layer are also in equilibrium. Substantial differences in boundary layer depth have developed at that point and both the subcloud and cloud layer are warmer and moister at stronger winds (Fig. 6). Because the surface fluxes remain different among U_5, U_{10}, and U_{15}, the subcloud layer θ and q evidently have not increased enough to offset the wind speed change.

At stronger winds, the larger moisture fluxes and larger (negative) heat fluxes throughout the cloud layer (Figs. 6e,f) reflect more moist and (potentially) cold air being mixed upward, as well as more dry and warm air being mixed downward. The profiles of F_b, $w_{\rm co}$, and buoyancy excess in cloud cores (Fig. 6g,j,l) show that updrafts are not more energetic at stronger winds, nor are clouds more numerous or mass fluxes larger (Figs. 6i,k). Because the mass fluxes are so similar, there is no evidence that E is larger at stronger winds. This can be seen from Eq. (9) where in equilibrium the left-hand side vanishes and E must balance $M - \overline{w}_{\eta}$. Because η and therefore $\overline{w}_{\eta}$ do not differ much, and neither does M, we can assume E is also not that different. This implies that the larger turbulent fluxes across the transition layer (the entrainment fluxes) are just the result of larger jumps in θ and q across the transition layer ($\Delta_{\eta}\theta$ and $\Delta_{\eta}q$). In other words, the cloud layer has warmed more and moistened less relative to the subcloud layer.

It is important to point out that the gradients of θ and q in the cloud layer are approximately constant with wind speed. The cloud layer consequently experiences similar large-scale drying and warming due to subsidence. In equilibrium, this constrains the divergence of the turbulent fluxes in the cloud layer [Eqs. (1) and (2)]. Differences in equilibrium surface fluxes at different wind speeds hence reflect the difference in fluxes at the inversion that develop (a point to which we return in the discussion).

4. An explanation for the deepening response from bulk theory

The simulations show that in the transient response to an increase in winds, a stronger moisture flux and mass flux into the inversion lead to a deepening of the cloud layer. These differences in boundary layer depth and in the surface moisture flux are maintained toward a new equilibrium. These observations, however, do not tell us if the layer needs to evolve in this way. Without the sudden increase of mass flux and liquid water into the inversion right after the perturbation, would the layer still have deepened? Do surface fluxes have to change with wind speed?

Using the bulk concepts introduced in section 2, we here explore whether from an energetic point of view the boundary layer h has to be deeper at stronger winds.

Because bulk models presume a certain structure in the cloud layer, this also explores the extent to which the detailed internal structure of the cloud layer (how clouds mix with the environment) matters in setting the new equilibrium. Our strategy is as follows: we explore whether a (consistent) new equilibrium can be obtained in which h has not changed. This is done for two hypothetical situations, one whereby equilibrium surface fluxes are constant with wind speed and one whereby they are not.

In developing our arguments we make use of Fig. 7, which displays a simplified vertical structure of the trade wind layer, similar to Fig. 1. The top panel (black dashed lines) shows the profiles of temperature and humidity and their corresponding fluxes before wind speed is perturbed. The subcloud layer is well mixed in θ_m and q_m. The subcloud layer depth is assumed to equal the saturation level. Jumps in temperature and humidity at the top of the subcloud layer (the transition layer) are ignored. The profiles are linear in the cloud layer with a discontinuity at h represented by $\Delta_h\theta$ and $\Delta_h q$.

The flux profiles are constructed by linearly relating the heat and moisture fluxes at h to their surface values, by using a flux difference across the layer equal to $\Delta F = F_s - F_h$:

$$F_{q,h} = F_{q,s} - \Delta F_q = C_D U(q_s - q_m) - \Delta F_q, \tag{11}$$

$$F_{\theta,h} = F_{\theta,s} - \Delta F_\theta = C_D U(\theta_s - \theta_m) - \Delta F_\theta, \tag{12}$$

where $\Delta F_\theta, \Delta F_q > 0$ and the surface fluxes $F_{\theta,s}$ and $F_{q,s}$ follow from bulk aerodynamic formulas [Eqs. (3) and (4)]. The buoyancy flux F_b at η follows from the common closure in which the flux at the top of the subcloud layer is a fixed fraction κ of its surface value:

$$F_{b,\eta} = \kappa F_{b,s}, \tag{13}$$

with $\kappa = -0.2$. The buoyancy flux is linearly extrapolated into the cloud layer where it represents the dry virtual potential temperature flux F_{b^*} (dashed lines) (Stevens 2007).

We can replace the moisture flux at h on the left-hand side of Eq. (11) by recognizing that in equilibrium it must balance the large-scale drying flux (due to subsidence). Similarly, the heat flux balances the large-scale warming flux and the radiative flux difference $Q_r\Delta h$ at h. When writing the large-scale drying and warming flux as the product of subsidence velocity and the jump of temperature and humidity across h, this gives

$$\overline{w}_h\Delta_h q = C_D U(q_s - q_m) - \Delta F_q, \tag{14}$$

$$\overline{w}_h\Delta_h\theta = C_D U(\theta_s - \theta_m) - \Delta F_\theta + Q_r\Delta h, \tag{15}$$

with $\overline{w}_h < 0, \Delta_h q < 0, \Delta_h\theta > 0$, and $Q_r\Delta h < 0$ (the latter vanishes for an infinitesimally thin inversion).

Now let us assume that U is perturbed by an amount of $\delta U > 0$. The profiles in red (two middle rows) in Fig. 7 resemble possible new equilibria in which the boundary layer depth has not changed. In the first situation the layer moistens enough by δq to offset the increased contribution of wind speed to the surface flux, so that $\delta F_q = 0$. In the second situation moistening is not enough and $\delta F_q \neq 0$. Note that in both situations we have kept the cloud layer gradients the same as in the top panel (before the perturbation), motivated by the simulations that show little change in cloud layer gradients with wind speed.

If $F_{q,s}$ does not change, and neither does ΔF_q (because the gradient of q does not change), then $F_{q,h}$ does not change either [Eq. (11)]. Such a situation, however, is inconsistent with the large-scale drying flux at h that has increased by an amount of $\overline{w}_h\delta q$:

$$\overline{w}_h(\Delta_h q - \delta q) \neq F_{q,h}. \tag{16}$$

This situation, whereby neither h nor the surface fluxes change with $\delta U > 0$, thus appears invalid.

In situation (2) we expect that $\delta F_q > 0$ if $\delta U > 0$, where δF_q is defined as

$$\delta F_q = C_D\delta U(q_s - q_m) - C_D U\delta_q. \tag{17}$$

Using this in Eq. (15) gives the new moisture flux balance at h:

$$\begin{aligned}\overline{w}_h(\Delta_h q - \delta q) &= F_{q,h} + \delta F_q \\ &= F_{q,h} + C_D\delta U(q_s - q_m) - C_D U\delta q \\ &= F_{q,h} + (\delta U/U)F_{q,s} - C_D U\delta q,\end{aligned} \tag{18}$$

which appears to be a consistent and plausible new equilibrium. The expression can be rearranged to solve for δq:

$$\delta q = \frac{F_{q,s}(\delta U/U)}{C_D U - \overline{w}_h}. \tag{19}$$

A similar derivation can be done for temperature, recalling that $\delta Q_r = 0$:

$$\delta\theta = \frac{F_{\theta,s}(\delta U/U)}{C_D U - \overline{w}_h}. \tag{20}$$

If we mimic the situation in LES where $F_{\theta,s} = 0$, this expression shows that $\delta\theta = 0$ [there is no change in the

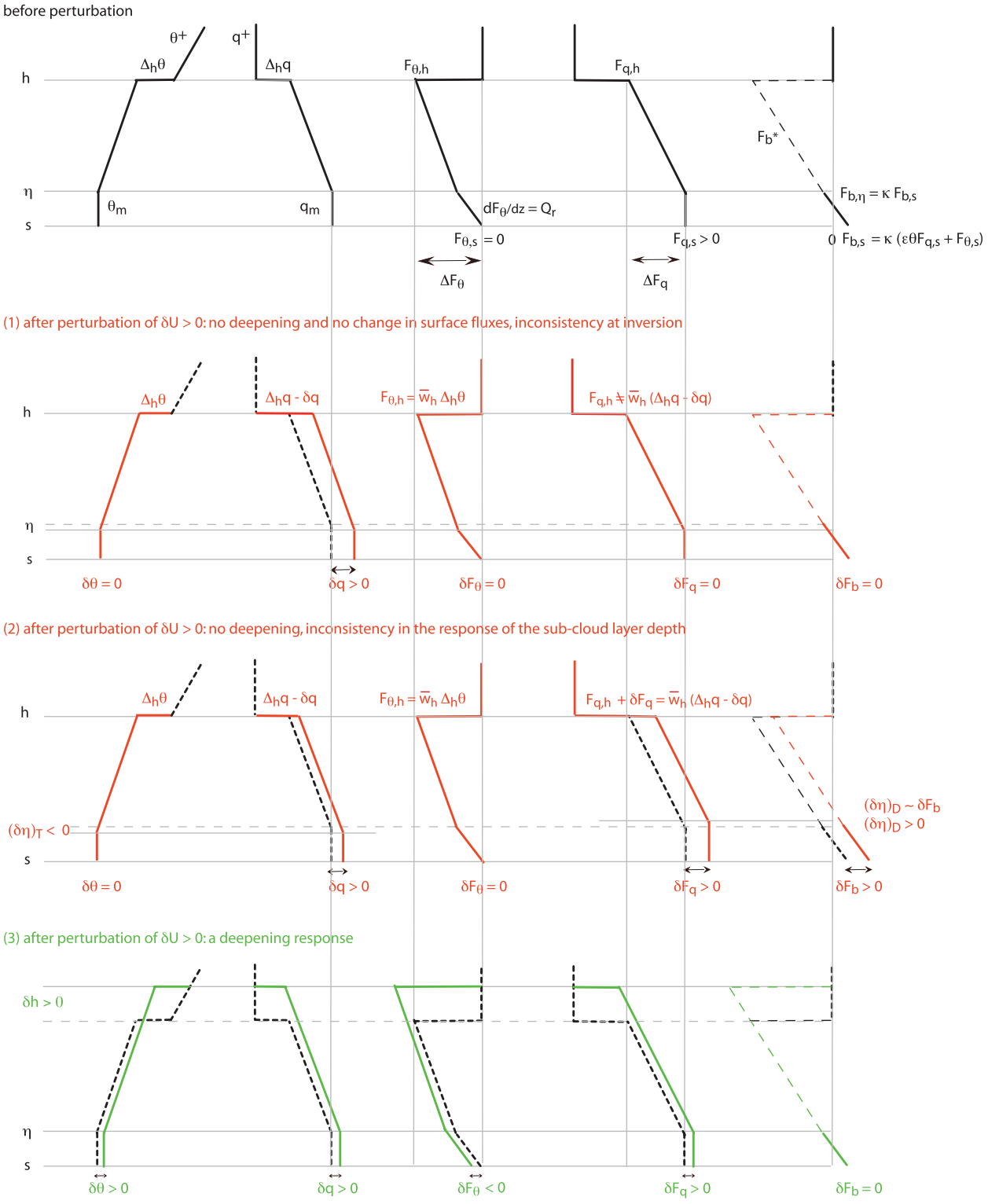

FIG. 7. Illustration of three possible responses to increasing wind speed ($\delta U > 0$). (row 1) The initial equilibrium state, here with $F_{\theta,s} = 0$. (from left to right) The profile of θ, q, F_θ, F_q, and F_b*. (rows 2–4) The three responses a new equilibrium without a deepening of the boundary layer, whereby 1) an inconsistency at the inversion develops, or 2) an inconsistency in the subcloud layer budget develops, and 3) a new equilibrium with the deepening response as observed in LES. The meaning of the different parameters and an explanation of the responses is outlined in section 4.

θ profile in Fig. 7 for situations (1) and (2)]. Remember that this is different from what we have seen in LES [situation (3), in green in Fig. 7], because we here assume that h does not change.

Equations (19) and (20) show that in general, because their denominator is positive, a situation with positive surface fluxes will lead to a net moistening and warming with an increase in wind speed. As long as δq and $\delta\theta$ at the surface equal δq and $\delta\theta$ at h (but the gradients dq/dz and $d\theta/dz$ can differ locally), the above is true.

We can note that the above expressions do not depend on η, but they do constrain it. Thermodynamically, η is controlled by maintaining a height close to the saturation level [Eq. (9) in section 3b], which in turn is controlled by subcloud layer humidity and temperature. In the case considered here, with $\delta\theta = 0$ and $\delta q > 0$, $(\delta\eta)_T < 0$, where we use T to denote the thermodynamic control on η.

This change in η is inconsistent with the changes that take place in the buoyancy budget of the subcloud layer. The divergence of F_b in the subcloud layer follows from the divergence of the heat and moisture flux. In equilibrium these are $dF_q/dz = 0$ and $dF_\theta/dz = Q_r$ [note that $d\theta/dz$ and dq/dz in the subcloud layer are zero; see also Eqs. (1) and (2)]:

$$\frac{dF_b}{dz} = \frac{F_{b,\eta} - F_{b,s}}{\eta} = Q_r, \tag{21}$$

where $Q_r < 0$. A similar budget equation was derived in Bretherton (1993). Using Eq. (13) this expression becomes

$$\kappa F_{b,s} = F_{b,s} + Q_r\eta. \tag{22}$$

In response to δU, the buoyancy flux changes by an amount of δF_b so that the new equilibrium is

$$\kappa(F_{b,s} + \delta F_b) = (F_{b,s} + \delta F_b) + Q_r(\eta + \delta\eta), \tag{23}$$

where we assume $\delta Q_r = 0$. This can be rewritten to

$$\kappa F_b = \delta F_b + Q_r\delta\eta, \tag{24}$$

which demonstrates that a situation in which the subcloud layer depth does not change with wind speed ($\delta\eta = 0$) can only be true if either $\kappa = 1$ or if $\delta F_b = 0$. In other words, if the subcloud layer depth does not change, the surface buoyancy flux cannot change and vice versa.

If $\delta\eta \neq 0$, however, we can write

$$(\delta\eta)_D = -\delta F_b\frac{1 - \kappa}{Q_r}, \tag{25}$$

where $(\delta\eta)_D$ refers to changes in subcloud layer depth that are constrained dynamically by variations in $F_{b,s}$. Replacing F_b with $F_\theta + \varepsilon\theta F_q$ [Eq. (5)] gives

$$(\delta\eta)_D = -[\delta F_\theta + \epsilon\theta\delta F_q]\frac{1 - \kappa}{Q_r}. \tag{26}$$

For the situation in LES ($F_{\theta,s} = 0$) Eq. (20) predicts that $\delta\theta = 0, \delta F_\theta = 0$, and $\delta F_q > 0$. Equation (26) then predicts that the subcloud layer depth must increase: $(\delta\eta)_D > 0$ (recall that both κ and $Q_r < 0$). This is opposite to $(\delta\eta)_T$.

This contradiction can be resolved by deepening the boundary layer as a whole [situation (3), in green in Fig. 7]. This increases the amount of warm and dry air from the overlying free troposphere that is mixed into the layer. The extra warming and drying causes the surface heat and moisture flux to respond oppositely, leading to $\delta F_{b,s} \approx 0$, and allows for $\delta\eta \approx 0$.

How do our findings depend on the assumption that the surface heat flux is zero when the perturbation takes place? If the analysis is performed for cases where $F_{\theta,s} > 0$ or < 0, similar contradictions arise. For instance, if $F_{\theta,s} < 0$, Eq. (20) predicts a cooling of the layer that tends to lower η just as moistening does, so that $(\delta\eta)_T < 0$. Equation (26), however, requires $(\delta\eta)_D = 0$ because of the opposite response of δF_θ and δF_q. In that situation an increase in h can also resolve the contradiction. Only when $F_{\theta,s} < 0$ as well as $F_{b,s} < 0$ initially, Eqs. (19), (20), and (25) predict that $\delta\eta < 0$. However, an initial buoyancy flux that is negative is rather unrealistic.

5. Discussion

Bulk concepts have shown that when the boundary layer does not deepen with an increase in wind speed, the subcloud layer depth experiences contradicting tendencies. Deepening the boundary layer as a whole may resolve this contradiction by increasing the amount of warm and dry air that is mixed toward the surface. Because this follows from a simple bulk model, it is suggested that the detailed internal structure of the cloud layer (how clouds mix with the environment) is only secondary to the deepening response.

The LES results in turn support the idea that how clouds mix with the environment does not change much with wind speed, because the temperature and humidity gradients in the cloud layer remain approximately the same. However, we may ask ourselves this question: if clouds had mixed the layer differently, could this have changed the deepening response to a nondeepening

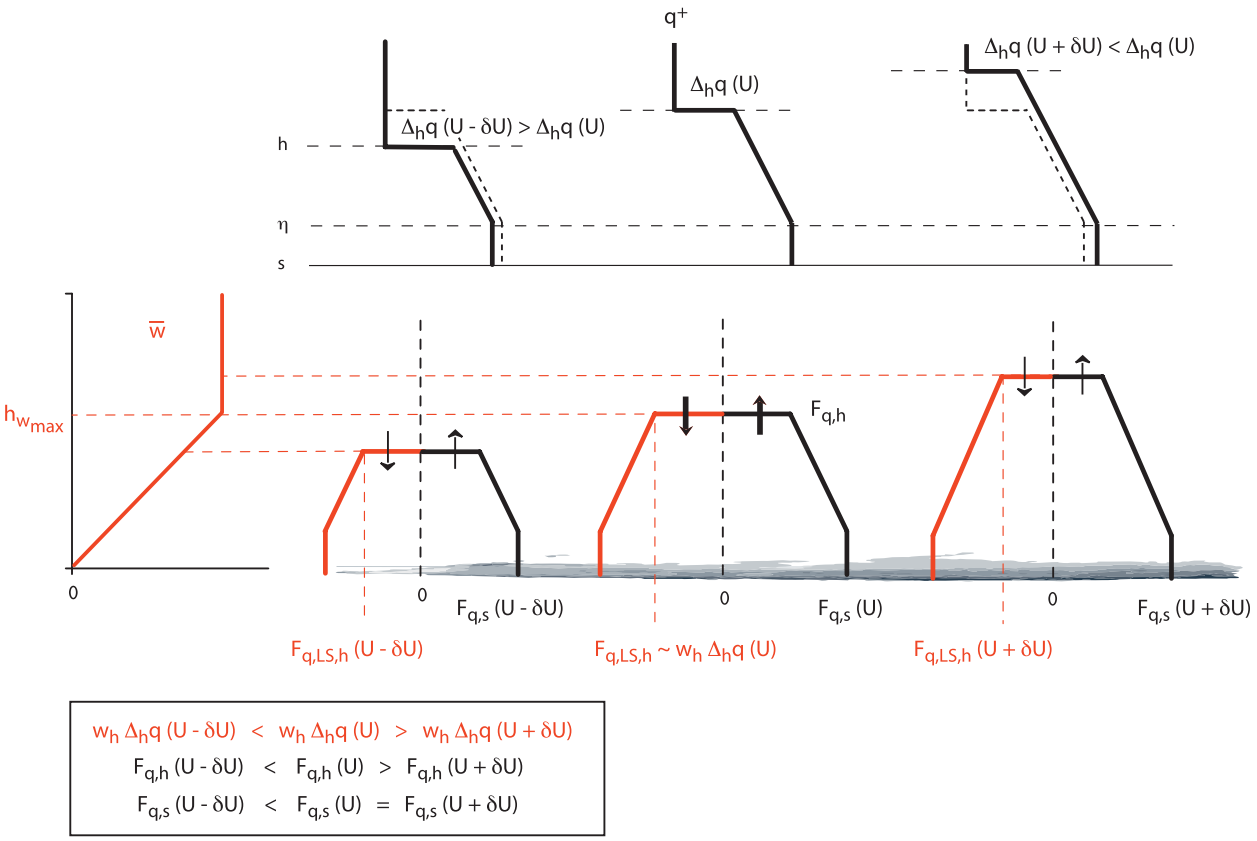

FIG. 8. Idealized sketch of the moisture balance at the inversion for different wind speeds, denoted by $U - \delta U$, U, and $U + \delta U$. (top) Simplified humidity profiles from Fig. 6. (bottom) Profiles of the turbulent moisture flux $F_{q,h}$ (black) and the large-scale drying flux $F_{q,\mathrm{LS}}$ (red). (bottom left) An idealized subsidence profile.

response? We could allow the gradients in Fig. 7 to change with wind speed, for instance by assuming that mixing at the bottom of the cloud layer is less efficient than at the top (not shown). We find, however, that the contradiction in the response of the subcloud layer depth remains.

The idea that how clouds mix with the environment does not change with a change in forcing (such as wind speed) is also used in the equilibrium model of Betts and Ridgway (1989), where bulk mixing line parameters are kept constant. This is done by fixing the partitioning between clear and cloudy air a priori, a parameter to which the surface fluxes and subcloud layer depth are found to be sensitive (Stevens 2006). Because we find that cloud fraction in LES does not vary much with wind speed, this may not be a bad assumption. BS12 show indeed that in equilibrium the bulk mixing line parameters (estimated from LES runs) are relatively insensitive to SST and free tropospheric temperature changes. The extent to which this is also true for wind speed and other large-scale forcings is an area of current research.

The simulations show that under stronger winds, stronger surface moisture fluxes are maintained toward a new equilibrium. The U_{15} simulation of case $S_{7.5}$, however, shows a somewhat different behavior, whereby the flux appears to relax back to its value at a 10 m s^{-1} wind speed (Fig. 5). We may explain this behavior using the same bulk concepts as earlier. In equilibrium, the turbulent moisture flux divergence must balance the large-scale drying [Eq. (2)], where we can write the latter ($\overline{w}d\overline{q}/dz$) as a flux divergence as well, $dF_{q,\mathrm{LS}}/dz$. Simplified profiles of F_q (black) and $F_{q,\mathrm{LS}}$ (red) are shown in the bottom panels of Fig. 8, which can be considered as generalizations of U_5, U_{10}, and U_{15} (Fig. 6f). This illustrates that in equilibrium the fluxes at the surface are related to F_q and $F_{q,\mathrm{LS}}$ at h and we here explore how the latter change with wind speed.

Because turbulent fluxes vanish in the free troposphere and the change in $F_{q,\mathrm{LS}}$ across h equals the product of the subsidence rate and the jump in q, the following balance is true at h:

$$F_{q,h} = \overline{w}_h \Delta_h q. \tag{27}$$

As the boundary layer from U_5 to U_{15} deepens, Δq_h decreases (top panels of Fig. 8) because the humidity

gradient in the free troposphere is zero. A simplified profile of $\overline{w}_h$, adapted from Fig. 2a, is sketched in red in the bottom-left panel of Fig. 8. Subsidence increases up to a certain height (which we call $h_{w_{\max}}$) and is constant above. The right-hand side of Eq. (27) can thus increase with wind speed, stay constant, or even decrease, depending on how h changes.

In U_{10}, for instance, $\overline{w}_h \Delta_h q$ is larger than in U_5. This implies larger turbulent moisture fluxes at all heights in the boundary layer, including at the surface, so that $F_{q,s}\,(U_5) < F_{q,s}\,(U_{10})$. Once h exceeds $h_{w_{\max}}$, as is true for U_{15}, $\overline{w}_h \Delta_h q$ can also decrease because of a decreasing Δq_h. In other words, at stronger winds less surface moisture flux is needed to satisfy the balance at h, which might explain why $F_{q,s}$ in U_{15} decreases throughout day 2 after the perturbation. This effect is not seen in the heat flux response because the free tropospheric temperature gradient is nonzero. The decrease in $F_{q,s}$ is also absent in the strongest wind speed case of the RICO simulations (not shown), likely because dq/dz is nonzero in that setup.

This analysis suggests that if a wind speed (or any) perturbation leads to a deepening of the boundary layer to a height where the large-scale drying flux is larger, the surface moisture fluxes in a new equilibrium may also be larger. If the large-scale drying flux decreases or remains constant with height, surface moisture fluxes may relax back to their original values. On longer time scales, the profile of the subsidence rate and the free tropospheric gradients of θ and q therefore become important constraints for the surface flux behavior.

The simulations we carried out are rather simplified in that they prescribe constant radiation, SST, and subsidence. Although the changes in these parameters along trade wind trajectories are important for the absolute response, even more relevant is how these forcings would covary with wind speed. For instance, we may hypothesize that a stronger large-scale circulation implies stronger trade winds as well as stronger subsidence, which would significantly reduce the deepening of the layer at strong winds compared to weak winds. We may also expect that stronger north–south SST gradients, present at times of stronger (zonal) surface wind speeds, relate to more wind shear (from the thermal wind equation) and therefore there is little difference in the depth of the layer over which easterly winds prevail.

It is also useful to consider the time period it takes to travel a certain distance X at weak U and strong $U + \delta U$ winds. The amount of deepening depends on the amount of moisture transported into the inversion, which is a function of the surface moisture flux and the time period traveled $T = X/U$. Using U_5 and U_{15} we may estimate this deepening as the tendency to deepen the layer $(dh/dt - \overline{w}_h)$ times T:

$$\frac{(dh/dt - \overline{w}_h)_{U+\delta U}}{(dh/dt - \overline{w}_h)_U}\frac{U}{U + \delta U} = \frac{10}{6} \times \frac{4}{8} = \frac{5}{6}, \quad (28)$$

which shows that differences in h between a near-equilibrium weak wind case and a near-equilibrium strong wind case, when observed at a single point downstream, are likely small (unless of course they are accompanied by changes in other parameters such as subsidence).

A last point of consideration is the neglect of rainfall in the simulations, which is known to reduce the deepening rate of the layer (Stevens 2007; Stevens and Seifert 2008; Van Zanten et al. 2011). Including rain likely reduces the differences in boundary layer depth between the different wind speed cases. Evaporation of rainfall within the subcloud layer in turn can lower the surface moisture flux and increase the surface heat flux. This effect on the surface fluxes may be further amplified by less deepening of the boundary layer when it rains more, which implies less warming and drying due to downward mixing of overlying free tropospheric air. Rainfall during RICO was on average 30 W m^{-2}, roughly half of the change in $F_{q,s}$ for δU = 3–5 m s^{-1}, so that rain effects may not be insignificant. Note that rainfall would bring the simulations closer to the observations, which show little change in the surface fluxes and less evident differences in boundary layer depth (Nuijens et al. 2009).

6. Conclusions

The influence of wind speed on shallow cumulus convection and the trade wind layer is explored using LES and bulk (equilibrium) concepts. Beginning with a basic state that is characteristic of the trades, and simplifying the issue by using constant SST, subsidence, and radiation, we find the following:

(i) The deepening of the cloud layer with a strengthening of the winds is a necessary part of the adjustment of the trade wind layer to a new equilibrium. The deepening resolves a contradiction in the response of the subcloud layer depth (cloud-base height) to a change in wind speed. Thermodynamically, an increase in wind speed tends to decrease subcloud layer depth if it is associated with the height at which parcels saturate. Dynamically, an increase in wind speed tends to increase subcloud layer depth if it is associated with the height at which the buoyancy flux falls to a fixed fraction of its surface value [Eq. (25)].

(ii) The adjustment toward a deeper cloud layer is accomplished by the transient response of the mass

flux, which initially increases with wind speed as the surface moisture flux increases. The deepening brings drier and warmer air to the surface, which maintains a larger input of moisture at the surface but reduces the surface sensible heat fluxes. The surface buoyancy fluxes are hence reduced and the initial increase in cloud-base mass fluxes is damped.

(iii) At stronger winds clouds are deeper but not more numerous or more energetic. This is because the equilibrium surface buoyancy flux varies little with wind speed, as the equilibrium surface heat and moisture flux respond in opposite ways to increasing winds.

(vi) The equilibrium response of the surface fluxes weakly depends on the thermodynamic structure of the free troposphere and the profile of subsidence.

(v) The temperature and humidity gradients in the cloud layer are approximately the same at different wind speeds, suggesting that how clouds are mixing the layer does not change with wind speed.

(vi) The need for deepening the cloud layer follows from simple bulk concepts, which suggests that the detailed internal structure of the layer (how clouds mix with the environment) is secondary to the deepening response.

A key finding of our work is that the equilibrium trade wind layer is deeper at stronger winds. Differences in the depth of the boundary layer however may be less apparent when observed at a single point downstream (assuming an equilibrium is reached). Larger wind speeds imply less travel time, hence less time to develop a deeper layer. Deeper clouds may also rain more along their way, limiting boundary layer growth. Moreover, as wind speed increases, shear becomes increasingly difficult to neglect and may mediate the further response of the layer. Another point worth investigating is whether wind speed generally covaries with subsidence or the thermodynamic structure of the free troposphere (i.e., whether other forcings associated with the large-scale circulation may either amplify or reduce the wind speed effect). Such interactions will determine whether the effect is felt not just locally, on cloud and boundary layer dynamics, but also deeper into the tropics, where it may feed back to the large-scale circulation.

When moving on to more realistic (and hence more complex) studies that focus on interactions among clouds, meteorology, and precipitation, the influence of wind speed on the aerosol and the microphysical development of clouds needs to be considered. Of relevance is the positive correlation between strong winds and concentrations of sea-salt aerosol that is attributed to sea spray from breaking waves (Clarke et al. 2003; Woodcock 1953). In addition, the apparent result that stronger winds correspond to stronger cloud-base updrafts during most of the RICO flights (Colón-Robles et al. 2006), a result for which we do not find evidence in our simulations, requires attention. Such an effect would influence peak supersaturation in moist updrafts and hence cloud droplet concentrations and rain formation.

The trades are a sensitive regime, in which small variations in the structure of the boundary layer as well as in the forces that act upon it may have significant effects. This may come as no surprise to the careful observer within the tropics, where small changes in the mean state of the atmosphere can be accompanied by substantial changes in the structure and organization of clouds and precipitation.

Acknowledgments. The authors wish to thank Gilles Bellon for sharing his modeling framework. Louise Nuijens thanks Chris Bretherton for his insightful suggestions on using a bulk equilibrium model to understand the deepening response to wind speed. Cathy Hohenegger and Juan-Pedro Mellado are thanked for many useful comments on an earlier draft version. The input of four critical reviewers substantially improved this manuscript. Simulations were performed at the Deutsches Klimarechenzentrum (DKRZ). This work was supported through NSF Grant ATM00342625 and by the Max Planck Institute for Meteorology in Hamburg, Germany.

REFERENCES

Back, L. E., and C. S. Bretherton, 2005: The relationship between wind speed and precipitation in the Pacific ITCZ. *J. Climate,* **18,** 4317–4328.

Bellon, G., and B. Stevens, 2012: Using the sensitivity of large-eddy simulations to evaluate atmospheric boundary layer models. *J. Atmos. Sci.,* in press.

Betts, A. K., 1973: Non-precipitating cumulus convection and its parameterization. *Quart. J. Roy. Meteor. Soc.,* **99,** 178–196.

——, and W. Ridgway, 1989: Climatic equilibrium of the atmospheric convective boundary layer over a tropical ocean. *J. Atmos. Sci.,* **46,** 2621–2641.

Bretherton, C. S., 1993: Understanding Albrecht's model of trade cumulus cloud fields. *J. Atmos. Sci.,* **50,** 2264–2283.

——, and S. Park, 2008: A new bulk shallow-cumulus model and implications for penetrative entrainment feedback on updraft buoyancy. *J. Atmos. Sci.,* **65,** 2174–2193.

——, M. E. Peters, and L. E. Back, 2004: Relationships between water vapor path and precipitation over the tropical oceans. *J. Climate,* **17,** 1517–1528.

Clarke, A., V. Kapustin, S. Howell, K. Moore, B. Lienert, S. Masonis, T. Anderson, and D. Covert, 2003: Sea-salt size distributions from breaking waves: Implications for marine aerosol production and optical extinction measurements during SEAS. *J. Atmos. Oceanic Technol.,* **20,** 1362–1374.

Colón-Robles, M., R. M. Rauber, and J. B. Jensen, 2006: Influence of low-level wind speed on droplet spectra near cloud base in trade wind cumulus. *Geophys. Res. Lett.,* **33,** L20814, doi:10.1029/2006GL027487.

Conzemius, R. J., and E. Federovich, 2006: Dynamics of sheared convective boundary layer entrainment. Part I: Methodological background and large-eddy simulations. *J. Atmos. Sci.,* **63,** 1151–1178.

Fairall, C. W., E. F. Bradley, J. E. Hare, A. A. Grachev, and J. B. Edson, 2003: Bulk parameterization of air–sea fluxes: Updates and verification for the COARE algorithm. *J. Climate,* **16,** 571–591.

Grant, A. L. M., and A. A. R. Brown, 1999: A similarity hypothesis for shallow-cumulus transports. *Quart. J. Roy. Meteor. Soc.,* **125,** 1913–1936.

Holloway, C. E., and J. D. Neelin, 2009: Moisture vertical structure, column water vapor, and tropical deep convection. *J. Atmos. Sci.,* **66,** 1665–1683.

Malkus, J. S., 1956: Trade cumulus cloud groups: Some observations suggesting a mechanism of their origin. *Tellus,* **9,** 33–44.

——, 1958: On the structure of the trade wind moist layer. *Pap. Phys. Oceanogr. Meteor.,* **13** (2), 1–46.

Matheou, G., D. Chung, L. Nuijens, B. Stevens, and J. Teixeira, 2011: On the fidelity of large-eddy simulation of shallow precipitating cumulus convection. *Mon. Wea. Rev.,* **139,** 2918–2939.

Medeiros, B., L. Nuijens, C. Antoniazzi, and B. Stevens, 2010: Low-latitude boundary layer clouds as seen by CALIPSO. *J. Geophys. Res.,* **115,** D23207, doi:10.1029/2010JD014437.

Moeng, C. H., and P. P. Sullivan, 1994: A comparison of shear and buoyancy-driven planetary boundary layer flows. *J. Atmos. Sci.,* **51,** 999–1022.

Neggers, R. A. J., B. Stevens, and J. D. Neelin, 2006: A simple equilibrium model for shallow-cumulus-topped mixed layers. *Theor. Comput. Fluid Dyn.,* **20,** 305–322.

Nuijens, L., B. Stevens, and A. P. Siebesma, 2009: The environment of precipitating shallow cumulus convection. *J. Atmos. Sci.,* **66,** 1962–1979.

Pino, D., J. Vilà-Guerau de Arellano, and P. G. Duynkerke, 2003: The contribution of shear to the evolution of a convective boundary layer. *J. Atmos. Sci.,* **60,** 1913–1926.

Savic-Jovcic, V., and B. Stevens, 2008: The structure and mesoscale organization of precipitating stratocumulus. *J. Atmos. Sci.,* **65,** 1587–1605.

Stevens, B., 2005: Atmospheric moist convection. *Annu. Rev. Earth Planet. Sci.,* **33,** 605–643.

——, 2006: Bulk boundary-layer concepts for simplified models of tropical dynamics. *Theor. Comput. Fluid Dyn.,* **20,** 279–304.

——, 2007: On the growth of layers of nonprecipitating cumulus convection. *J. Atmos. Sci.,* **64,** 2916–2931.

——, and A. Seifert, 2008: Understanding macrophysical outcomes of microphysical choices in simulations of shallow cumulus convection. *J. Meteor. Soc. Japan,* **86,** 143–162.

Van Zanten, M. C., and Coauthors, 2011: Controls on precipitation and cloudiness in simulations of trade-wind cumulus as observed during RICO. *J. Adv. Model. Earth Syst.,* **3,** M06001, doi:10.1029/2011MS000056.

Woodcock, A. H., 1953: Salt nuclei in marine air as a function of altitude and wind force. *J. Meteor.,* **10,** 362–371.